Focused blind deconvolution

Pawan Bharadwaj*, Laurent Demanet, and Aimé Fournier
Massachusetts Institute of Technology

Abstract—We introduce a novel multichannel blind deconvolution (BD) method that extracts *sparse* and *front-loaded* impulse responses from the channel outputs, i.e., their convolutions with a single arbitrary source. A crucial feature of this formulation is that it doesn't encode support restrictions on the unknowns, unlike most prior work on BD. The indeterminacy inherent to BD, which is difficult to resolve with a traditional ℓ_1 penalty on the impulse responses, is resolved in our method because it seeks a first approximation where the impulse responses are: "maximally white" — encoded as the energy focusing near zero lag of the impulse-response auto-correlations; and "maximally front-loaded" — encoded as the energy focusing near zero time of the impulse responses. Hence we call the method focused blind deconvolution (FBD). The focusing constraints are relaxed as the iterations progress. Note that FBD requires the duration of the channel outputs to be longer than that of the unknown impulse responses.

A multichannel blind deconvolution problem that is appropriately formulated by sparse and front-loaded impulse responses arises in seismic inversion, where the impulse responses are the Green's function evaluations at different receiver locations, and the operation of a drill bit inputs the noisy and correlated source signature into the subsurface. We demonstrate the benefits of FBD using seismic-while-drilling numerical experiments, where the noisy data recorded at the receivers are hard to interpret, but FBD can provide the processing essential to separate the drill-bit (source) signature from the interpretable Green's function.

Index Terms—Blind deconvolution, seismic interferometry, phase retrieval, channel identification, dereverberation, front-loaded, coprime.

I. INTRODUCTION

There are situations where seismic experiments are to be performed in environments with a noisy source e.g., when an operating borehole drill is loud enough to reach the receivers. The source generates an unknown, noisy signature $s(t)$ at time t; one typically fails to dependably extract the source signature despite deploying an attached receiver. For example, the exact signature of the operating drill bit in a borehole environment cannot be recorded because there would always be some material interceding before the receiver [1]. The noisy-source signals propagate through the subsurface, and result in the data at the receivers, denoted by $d_i(t)$. Imaging of the data to characterize the subsurface (seismic inversion) is only possible when they are deconvolved to discover the subsurface Green's function. Similarly, in room acoustics, the speech signals $s(t)$ recorded as $d_i(t)$ at a microphone array are distorted and sound reverberated due to the reflection of walls, furniture and other objects. Speech recognition and compression is simpler when the reverberated records $d_i(t)$ at the microphones are deconvolved to recover the clean speech signal [2], [3].

The response of many such physical systems to a noisy source is to produce multichannel outputs. The n observations or channel outputs, in the noiseless case, are modeled as the output of a linear system that convolves (denoted by $*$) a source (with signature $s(t)$) with the impulse response function:

$$d_i(t) = \{s * g_i\}(t). \tag{1}$$

Here, $g_i(t)$ is the ith channel impulse response and $d_i(t)$ is the ith channel output. The impulse responses contain physically meaningful information about the channels. Towards the goal of extracting the vector of impulse responses $[g_1(t), \ldots, g_n(t)]$ or simply $[g_i]$ and the source function $s(t)$, we consider an unregularized least-squares fitting of the channel-output vector $[d_1(t), \ldots, d_n(t)]$ or $[d_i]$. This corresponds to the least-squares multichannel deconvolution [4]–[6] of the channel outputs with an unknown blurring kernel, i.e., the source signature. It is well known that severe non-uniqueness issues are inherent to multichannel blind deconvolution (BD); there could be many possible estimates of $[g_i]$, which when convolved with the corresponding s will result in the recorded $[d_i]$ (as formulated in (6) below).

Therefore, in this paper, we add two additional constraints to the BD framework that seek a solution where $[g_i]$ are:

1) *maximally white* — encoded as the energy focusing near zero lag (i.e., energy diminishing at non-zero lags) of the impulse-response auto-correlations and
2) *maximally front-loaded* — encoded as the energy focusing near zero time of the most front-loaded impulse response.

We refer to them as *focusing* constraints. They are not equivalent to ℓ_1 minimization,* although they also enforce a form of sparsity. These are relaxed as the iterations progress to enhance the fitting of the channel outputs. Focused blind deconvolution (FBD) employs the focusing constraints to resolve the indeterminacy inherent to the BD problem. We identify that it is more favorable to use the constraints in succession after decomposing the BD problem into two separate least-squares optimization problems. The first problem, where it is sufficient to employ the first constraint, fits the *interferometric or cross-correlated* channel outputs [7], rather than the raw outputs, and solves for the inter-ferometric impulse response. The second problem relies on the outcome of the previous problem and completes FBD by employing the second constraint and solving for the impulse responses from their cross-correlations. This is shown in the Fig. 1. According to our numerical experiments, FBD can effectively retrieve $[g_i]$ provided the following conditions are met:

---

*That is, minimizing $\sum_t |g_i(t)|$ to promote sparsity.

- the duration length of the unknown impulse responses should be much briefer than that of the channel outputs;
- the channels are *sufficiently dissimilar* in the sense of their transfer-function polynomials being *co-prime* in the z-domain.

In the seismic inversion context, the first condition is economically beneficial, as usual drilling practice enables us to record noisy data for a time period much longer compared to the wave-propagation time. Also, since drilling is anyway necessary, its use as a signal source to estimate $[g_i]$ is a free side benefit. We show that the second condition can be satisfied in the seismic experiments by deploying *sufficiently dissimilar* receivers, as defined below, which may yet be arrayed variously in a borehole, or surface-seismic geometry.

It is shown in [8] that multichannel blind deconvolution is dependent on the condition that the transfer functions are coprime, i.e., they do not share common roots in the z-domain. The BD algorithms in [9], [10] are also based on this prerequisite. In this regard, due to the difficulty of factoring the high order channel polynomials, [11] proposed a method for identification of common roots of two channel polynomials. Interestingly, they have observed that the roots do not have to be exactly equal to be considered common in BD. Khong et al. [12] uses clustering to efficiently extract clusters of near-common roots. In contrast to these methods, FBD doesn't need the identification of the common roots of the channel polynomials.

Surveys of BD algorithms in the signal and image processing literature are given in [13], [14]. A series of results on blind deconvolution appeared in the literature using different sets of assumptions on the unknowns. The authors in [15], [16] show that BD can be efficiently solved under certain subspace conditions on both the source signature and impulse responses even in the single-channel case. [17] showed the recovery of the unknowns in multichannel BD assuming that the source is sparse in some known basis and the impulse responses belong to known random subspaces. The experimental results in [18] show the successful joint recovery of Gaussian impulse responses with known support that are convolved with a single Gaussian source signature. BD algorithms with various assumptions on input statistics are proposed in [19]–[21]. Compared to the work in these articles, FBD doesn't require any assumptions on 1) support of the unknowns, 2) statistics of the source signature and 3) the underlying physical models;[†] although, it does apply a type of sparsity prior on the $[g_i]$. Note also that regularization in the sense of minimal ℓ_1 i.e., mean-absolute norm, as some methods employ, does not fully address the type of indeterminacy associated with BD.

Deconvolution is also an important step in the processing workflow used by exploration geophysicists to improve the resolution of the seismic records [23]–[25]. Robinson [26] developed predictive decomposition

[27] of the seismic record into a source signature and a white or uncorrelated time sequence corresponding to the Earth's impulse response. In this context, the impulse responses $[g_i]$ correspond to the unique subsurface Green's function $g(\vec{x}, t)$ evaluated at the receiver locations $[\vec{x}_i]$, where the seismic-source signals are recorded. Spiking deconvolution [28], [29] estimates a Wiener filter that increases the *whiteness* of the seismic records, therefore, removing the effect of the seismic sources. In order to alleviate the non-uniqueness issues in blind deconvolution, recent algorithms in geophysics:

- take advantage of the multichannel nature of the seismic data [30]–[33];
- sensibly choose the initial estimates of the $[g_i]$ in order to converge to a desired solution [33]; and/or
- constrain the sparsity of the $[g_i]$ [31].

Kazemi et al. [34] used sparse BD to estimate source and receiver wavelets while processing seismic records acquired on land. The BD algorithms in the current geophysics literature handle roughly impulsive source wavelets that are due to well-controlled sources, as opposed to the noisy and uncontrollable sources in FBD, about which we assume very little. It has to be observed that building initial estimates of the $[g_i]$ is difficult for any algorithm, as the functional distances between the $[d_i]$ and the actual $[g_i]$ are quite large. Unlike standard methods, FBD does not require an extrinsic starting guess.

The Green's function retrieval is also the subject of *seismic interferometry* [35]–[40], where the cross-correlation (denoted by $\otimes$) between the records at two receivers with indices i and j,

$$d_{ij}(t) = \{d_i \otimes d_j\}(t) = \{s_{\mathrm{a}} * g_{ij}\}(t), \qquad (2)$$

is treated as a proxy for the cross-correlated or *interferometric* Green's function $g_{ij} = g_i \otimes g_j$. A classic result in interferometry states that a summation on the g_{ij} over various noisy sources, evenly distributed in space, will result in the Green's function due to a *virtual source* at one of the receivers [41]. In the absence of multiple evenly distributed noisy sources, the interferometric Green's functions can still be directly used for imaging [42]–[46], although this requires knowledge of the source signature. The above equation shows that the goal of interferometry, i.e., construction of g_{ij} given d_{ij}, is impeded by the source auto-correlation $s_{\mathrm{a}} = s \otimes s$. In an impractical situation with a zero-mean white noisy source, the d_{ij} would be precisely proportional to g_{ij}; but this is not at all realistic, so we don't assume a white source signature in FBD and eschew any concepts like virtual sources.

The failure of seismic noisy sources to be white[‡] is already well known in seismic interferometry [39], [50]. To extract the response of a building, [51] propose a deconvolution of the recorded waves at different locations in the building rather than the cross-correlation. Seismic interferometry by multi-dimensional deconvolution [52]–[55] uses an estimated interferometric point

---

[†] Some seismic BD algorithms design deconvolution operators using an estimated subsurface velocity model [22].

[‡] For example, the noise generated by drill bit operations is heavily correlated in time [47]–[49].

spread function as a deconvolution operator. The results obtained from this approach depend on the accuracy of the estimated point spread function, which relies on a uniform distribution of multiple noisy sources in space. In contrast to these seismic-interferometry-by-deconvolution approaches, FBD is designed to perform a *blind* deconvolution in the presence of a single noisy source and doesn't assume an even distribution of the noisy sources. In the presence of multiple noisy sources, as preprocessing to FBD, one has to use seismic blind source separation. For example, [56], [57] used independent component analysis for convolutive mixtures to decompose the multi-source recorded data into isolated records involving one source at a time.

The remainder of this paper is organized as follows. We explain the indeterminacy of unregularized BD problem in section II. In section III, we introduce FBD and argue that it can resolve this indeterminacy. This paper contains no theoretical guarantee, but we regard the formulation of such theorems as very interesting. In section IV, we demonstrate the benefits of FBD using both idealized and practical synthetic seismic experiments.

II. MULTICHANNEL BLIND DECONVOLUTION

The z-domain representations are denoted in this paper using the corresponding capital letters. For example, the ith channel output after a z-transform is denoted by

$$D_i(z) = \sum_{t=0}^{T} d_i(t) z^{-t}.$$

The traditional algorithmic approach to solve BD is a least-squares fitting of the channel output vector $[d_i : \{0, \ldots, T\} \to \mathbb{R}]$ to jointly optimize two functions i.e., the impulse response vector associated with different channels $[g_i : \{0, \ldots, \tau\} \to \mathbb{R}]$ and the source signature $s : \{0, \ldots, T\} \to \mathbb{R}$. The joint optimization can be suitably carried out using alternating minimization [58], [59]: in one cycle, we fix one function and optimize the other, and then fix the other and optimize the first. Several cycles are expected to be performed to reach convergence.

Definition 1 (LSBD: Least-squares Blind Deconvolution). It is a basic formulation that minimizes the least-squares functional:

$$U(s, [g_i]) = \sum_{k=1}^{n} \sum_{t=0}^{T} \{d_k(t) - \{s * g_k\}(t)\}^2; \quad (3)$$

$$(\hat{s}, [\hat{g}_i]) = \underset{s, [g_i]}{\arg\min} \quad U \quad (4)$$

$$\text{subject to} \quad \sum_{t=0}^{T} s^2(t) = 1. \quad (5)$$

Here, $\hat{s}$ and $[\hat{g}_i]$ denote the predicted or estimated functions corresponding to the unknowns s and $[g_i]$, respectively. We have fixed the energy (i.e., sum-of-squares) norm of s in order to resolve the scaling ambiguity. In order to effectively solve this problem,
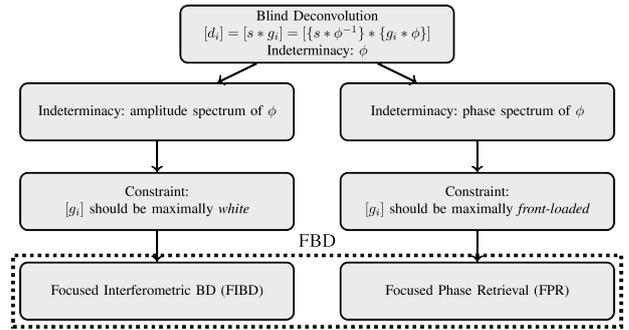
Figure 1: Focused blind deconvolution uses two focusing constraints to resolve the indeterminacies of the multichannel blind deconvolution. Note that this is not an algorithmic flowchart, but explains the two components of the regularization in FBD.

it is required that the domain length $T + 1$ of the first unknown function s be longer than the domain length $\tau + 1$ of the second unknown function $[g_i]$ [8].

Ill-posedness is the major challenge of BD, irrespective of the number of channels. For instance, when the number of channels $n = 1$, an undesirable minimizer for (3) would be the temporal Kronecker $\delta(t)$ for the impulse response, making the source signature equal the channel output. Even with $n \geq 1$, the LSBD problem can only be solved up to some indeterminacy. To quantify the ambiguity, consider that a filter $\phi(t) \neq \delta(t)$ and its inverse $\phi^{-1}(t)$ (where $\phi * \phi^{-1} = \delta$) can be applied to each element of $[g_i]$ and s respectively, and leave their convolution unchanged:

$$d_i(t) = \{s * g_i\}(t) = \{\{s * \phi^{-1}\} * \{g_i * \phi\}\}(t). \quad (6)$$

If furthermore $s * \phi^{-1}$ and $[g_i * \phi]$ obey the constraints otherwise placed on s and $[g_i]$, namely in our case that s and $[g_i]$ should have duration lengths $T + 1$ and $\tau + 1$ respectively, and the unity of the source energy, then we are in presence of a true ambiguity not resolved by those constraints. We then speak of ϕ as belonging to a set $\mathbb{Q}$ of undetermined filters. This formalizes the lack of uniqueness [8]: for any possibly desirable solution $(\hat{s}, [\hat{g}_i])$ and every $\phi \in \mathbb{Q}$, $(\hat{s} * \phi^{-1}, [\hat{g}_i * \phi])$ is an additional possibly undesirable solution. Taking all $\phi \in \mathbb{Q}$ spawns all solutions in a set $\mathbb{P}$ that equally minimize the least-squares functional in (3). Accordingly, in the z-domain, the elements in $[\hat{G}_i]$ of almost any solution in $\mathbb{P}$ share some common root(s), which are associated with its corresponding unknown filter $\Phi(z)$. In other words, the channel polynomials in $[\hat{G}_i]$ of nearly all the solutions are *not coprime*. A particular element in $\mathbb{P}$ has its corresponding $[\hat{G}_i]$ with the fewest common roots — we call it the *coprime* solution.

III. FOCUSED BLIND DECONVOLUTION

The aim of focused blind deconvolution is to seek the coprime solution of the LSBD problem. Otherwise, the

channel polynomials $[\hat{G}_i]$ will typically be *less sparse* and *less front-loaded* in the time domain owing to the common roots that are associated with the undetermined filter ϕ of (6). For example, including a common root r to the polynomials in $[\hat{G}_i]$ implies an additional factor $(z - r)$ that corresponds to subtracting $[r\, g_i(t)]$ from $[g_i(t + 1)]$ in the time domain, so that the sparsity is likely to reduce. Therefore, the intention and key innovation of FBD is to minimize the number of common roots in the channel polynomials $[\hat{G}_i]$ associated with $\Phi(z)$. It is difficult to achieve the same result with standard ideas from sparse regularization.

Towards this end, focused blind deconvolution solves a series of two least-squares optimization problems with focusing constraints. These constraints, described in the following subsections, can guide FBD to converge to the desired coprime solution. Note that this prescription does not guarantee that the recovered impulse responses should consistently match the true impulse responses;[§] nevertheless, we empirically encounter a satisfactory recovery in most practical situations of seismic inversion, as discussed below.

The first problem considers fitting the cross-correlated channel outputs to jointly optimize two functions i.e., the impulse-response cross-correlations $[g_{ij}]$ between every possible channel pair and the source-signature auto-correlation s_{a}. The focusing constraint in this problem will resolve the indeterminacy due to the amplitude spectrum of the unknown filter ϕ in (6) such that the impulse responses $[g_i]$ are *maximally white*. Then the second problem completes the focused blind deconvolution by fitting the above-mentioned impulse-response cross-correlations, to estimate $[g_i]$ from $[g_{ij}]$. The focusing constraint in this problem will resolve the indeterminacy due to the phase spectrum of the unknown filter ϕ such that the impulse responses $[g_i]$ are *maximally front-loaded*. As shown in the Fig. 1, these two problems will altogether resolve the indeterminacies of BD discussed in the previous section.

A. Focused Interferometric Blind Deconvolution

In order to isolate and resolve the indeterminacy due to the amplitude spectrum of $\phi(t)$, we consider a reformulated multichannel blind deconvolution problem. This reformulation deals with the cross-correlated or interferometric channel outputs, $d_{ij} : \{-T, \ldots, T\} \to \mathbb{R}$, as in (2), between every possible channel pair (cf. [45]), therefore ending the indeterminacy due to the phase spectrum of $\phi(t)$.

Definition 2 (IBD: Interferometric Blind Deconvolution). We use this problem to lay the groundwork for the next problem, and benchmarking. The optimization is carried out over the source-signature auto-correlation

---

[§]In the seismic context, FBD does not guarantee that the recovered Green's function satisfies the wave equation with impulse source.

$s_{\mathrm{a}} : \{-T, \ldots, T\} \to \mathbb{R}$ and the cross-correlated or interferometric impulse responses $g_{ij} : \{-\tau, \ldots, \tau\} \to \mathbb{R}$:

$$V(s_{\mathrm{a}}, [g_{ij}]) = \sum_{k=1}^{n} \sum_{l=k}^{n} \sum_{t=-T}^{T} \{d_{kl}(t) - \{s_{\mathrm{a}} * g_{kl}\}(t)\}^2; \tag{7}$$

$$(\hat{s}_{\mathrm{a}}, [\hat{g}_{ij}]) = \underset{s_{\mathrm{a}}, [g_{ij}]}{\arg\min} \quad V \tag{8}$$

$$\text{subject to} \quad s_{\mathrm{a}}(0) = 1; \quad s_{\mathrm{a}}(t) = s_{\mathrm{a}}(-t).$$

Here, we denoted the $(n + 1)n/2$-vector of unique interferometric impulse responses $[g_{11}, g_{12}, \ldots, g_{22}, g_{23}, \ldots, g_{nn}]$ by simply $[g_{ij}]$. We fit the interferometric outputs d_{ij} after max normalization. The motivation of conveniently fixing $s_{\mathrm{a}}(0)$ is not only to resolve the scaling ambiguity but also to converge to a solution, where the necessary inequality condition $s_{\mathrm{a}}(t) \leq s_{\mathrm{a}}(0) \,\forall\, t$ is satisfied. More generally, the function $s_{\mathrm{a}}(t)$ is the autocorrelation of $s(t)$ if and only if the Toeplitz matrix formed from its translates is positive semidefinite, i.e., Toeplitz$(s_{\mathrm{a}}) \succeq 0$. This is a result known as Bochner's theorem. This semidefinite constraint can be realized by projecting Toeplitz(s_{a}) onto the cone of positive semidefinite matrices at each iteration of the nonlinear least-squares iterative method [60]. Nonetheless, in the numerical experiments, we observe convergence to acceptable solutions by just using the weaker constraints of IBD, when is data noise is sufficiently small.

Similar to LSBD, IBD has unwanted minimizers obtained by applying a filter ψ^{-1} to s_{a} and ψ to each element of $[g_{ij}]$, but it is easily computed that ψ has to be *real and nonnegative* in the frequency domain $(|z| = 1)$ and related to the amplitude spectrum of $\phi(t)$. Therefore, its indeterminacy is lesser compared to that of the LSBD approach.

Definition 3 (FIBD: Focused Interferometric Blind Deconvolution). FIBD starts by seeking a solution of the underdetermined IBD problem where the impulse responses are "maximally white", as measured by the concentration of their autocorrelation near zero lag. Towards that end, we use a regularizing term that penalizes the energy of the impulse-response auto-correlations proportional to the non-zero lag time t, before returning to solving the regular IBD problem.

$$W(s_{\mathrm{a}}, [g_{ij}]) = V(s_{\mathrm{a}}, [g_{ij}]) + \alpha \sum_{k=1}^{n} \sum_{t=-\tau}^{\tau} t^2 g_{kk}^2(t); \tag{9}$$

$$(\hat{s}_{\mathrm{a}}, [\hat{g}_{ij}]) = \underset{s_{\mathrm{a}}, [g_{ij}]}{\arg\min} \quad W \tag{10}$$

$$\text{subject to} \quad s_{\mathrm{a}}(0) = 1; \quad s_{\mathrm{a}}(t) = s_{\mathrm{a}}(-t).$$

Here, $\alpha > 0$ is a regularization parameter. We consider a homotopy [61] approach to solve FIBD, where (10) is solved in succession for decreasing values of α, the result obtained for previous α being used as an initializer for the cycle that uses the current α. The focusing constraint resolves the indeterminacy of IBD.

Minimizing the energy of the impulse-response auto-correlations $[g_{ii}]$ proportional to the non-zero lag time will result in a solution where the impulse responses are heuristically as white as possible. In other words, FIBD minimizes the number of common roots, associated with the IBD indeterminacy $\Psi(z)$, in the estimated polynomials $[\hat{G}_{ij}]$, facilitating the goal of FBD to seek the coprime solution. The entire workflow of FIBD is shown in the Algorithm 1. In most of the numerical examples, we simply choose $\alpha = \infty$ first, and then $\alpha = 0$.

B. Focused Phase Retrieval

FIBD resolves a component of the LSBD ambiguity and estimates the interferometric impulse responses. This should be followed by phase retrieval (PR) — a least-squares fitting of the interferometric impulse responses $[\hat{g}_{ij}]$ to optimize the impulse responses $[g_i]$. The estimation of $[g_i]$ in PR is hindered by the unresolved LSBD ambiguity due to the phase spectrum of $\phi(t)$. In order to resolve the remaining ambiguity, we use a focusing constraint in PR.

Definition 4 (LSPR: Least-squares Phase Retrieval). Given the interferometric impulse responses $[g_{ij}]$, the aim of the phase retrieval problem is to estimate unknown $[g_i]$.

$$X([g_i]) = \sum_{k=1}^{n} \sum_{l=i}^{n} \sum_{t=-\tau}^{\tau} \{\hat{g}_{kl}(t) - \{g_k \otimes g_l\}(t)\}^2; \quad (11)$$

$$[\hat{g}_i] = \underset{[g_i]}{\arg\min} \quad X \quad (12)$$

LSPR is ill-posed. Consider a *white* filter $\chi(t) \neq \delta(t)$, where $\chi \otimes \chi = \delta$, that can be applied to each of the impulse responses, and leave their cross-correlations unchanged:

$$g_{ij}(t) = \{g_i \otimes g_j\}(t) = \{\{g_i * \chi\} \otimes \{g_j * \chi\}\}(t). \quad (13)$$

If furthermore $g_i * \chi$ obeys the constraint otherwise placed, namely in our case that the impulse responses should have duration length τ, then we are in the presence of a true ambiguity not resolved by this constraint. It is obvious that the filter $\chi(t)$ is linked to the remaining unresolved component of the LSBD indeterminacy, i.e., the phase spectrum of $\phi(t)$.

Definition 5 (FPR: Focused Phase Retrieval). FPR seeks a solution of the underdetermined LSPR problem where the impulse responses $[g_i]$ are "maximally front-loaded". It starts with an optimization that fits the interferometric impulse responses only linked with the most front-loaded channel[¶] f, before returning to solving the regular LSPR problem. We use a regularizing term that

---

[¶] In the seismic context, the most front-loaded channel corresponds to the closest receiver $i = f$ to the noisy source, assuming that the traveltime of the waves propagating from the source to this receiver is the shortest.

penalizes the energy of the most front-loaded response g_f proportional to the time $t \neq 0$:

$$Y([g_i]) = \sum_{k=1}^{n} \sum_{t=-\tau}^{\tau} \{\hat{g}_{kf}(t) - \{g_k \otimes g_f\}(t)\}^2$$

$$+ \beta \sum_{t=0}^{\tau} g_f^2(t) t^2; \quad (14)$$

$$[\hat{g}_i] = \underset{g_i}{\arg\min} \quad Y. \quad (15)$$

Here, $\beta \geq 0$ is a regularization parameter. Again, we consider a homotopy approach to solve this optimization problem, where the above equation is solved in succession for decreasing values of β. FPR chooses the undetermined filter χ such that $g_i * \chi$ has the energy maximally concentrated or focused at the front (small t). Minimizing the second moment of the squared impulse responses will result in a solution where the impulse responses are as front-loaded as possible. The entire workflow of FPR is shown in the Algorithm 2. In all the numerical examples, we simply choose $\beta = \infty$ first, and then $\beta = 0$. Counting on the estimated impulse responses from FPR, we return to the LSBD formulation in order to finalize the BD problem.

C. Sufficiently Dissimilar Channel Configuration

FBD seeks the coprime solution of the ill-posed LSBD problem. Therefore, for the success of FBD, it is important that the true transfer functions do not share any common zeros in the z-domain. This requirement is satisfied when the channels are chosen to be *sufficiently dissimilar*. The channels are said to be sufficiently dissimilar unless there exists a spurious γ and $[g_i]$ such that the true impulse-response vector $[g_i^0] = [\gamma * g_i]$. Here, γ is a filter that 1) is independent of the channel index i; 2) belongs to the set $\mathbb{Q}$ of filters that cause indeterminacy of the LSBD problem; 3) doesn't simply shift g_i in time. In our experiments, FBD reconstructs a good approximation of the true impulse responses if the channels are sufficiently dissimilar. Otherwise, FBD outputs an undesirable solution $(s^0 * \gamma^{-1}, [g_i])$, as opposed to the desired $(s^0, [\gamma * g_i])$, where s^0 is the true source signature. In the next section, we will show numerical examples with both similar and dissimilar channels.

IV. NUMERICAL SIMULATIONS

A. Idealized Experiment I

We consider an experiment with $n = 20$, $\tau = 30$ and $T = 400$. The aim is to reconstruct the true impulse responses $[g_i^0]$, plotted in Fig. 2a, from the channel outputs generated using a Gaussian random source signature s^0. The impulse responses of similar kind are of particular interest in seismic inversion and room acoustics as they reveal the arrival of energy, propagated from an impulsive source, at the receivers in the medium. In this case, the arrivals have onsets of 6 s and 10 s at the first channel and they curve linearly and hyperbolically, respectively. The linear arrival is

Algorithm 1: Focused Interferometric Blind Deconvolution. Alternating minimization of W, as in eq. 10, is carried out in succession for decreasing values of α.

Preparation
    generate the cross-correlated or interferometric channel outputs $[d_{ij}]$ and normalize with $d_{11}(0)$

Parameters (with example)
    tolerance for convergence $\epsilon = 10^{-8}$
    $\vec{\alpha} = \{\infty, 0\}$

Initialize
$$s_{\mathrm{a}}(t) \leftarrow \begin{cases} 0, & \text{if } t \neq 0 \\ 1, & \text{otherwise} \end{cases}$$
$$g_{ij}(t) \leftarrow \begin{cases} 0, & \text{if } i = j \text{ and } t \neq 0 \\ \mathrm{rand}(), & \text{otherwise} \end{cases}$$

Results
    interferometric transfer functions $[\hat{g}_{ij}]$
    autocorrelation for the source signature $\hat{s}_a$

Kernel
foreach $\alpha \in \vec{\alpha}$ **do**   /* loop over decreasing α */
1 | $W_1 = \infty$; $W_2 = \infty$; $W_{1p} = W_1$; $W_{2p} = W_2$; $\Delta W = \infty$
2 | **while** $\Delta W > \epsilon$ **do**
3 | | $s_a \leftarrow \underset{s_a}{\arg\min}\, W(s_{\mathrm{a}}, [g_{ij}])$ s.t. $s_{\mathrm{a}}(0) = 1$ & $s_{\mathrm{a}}(t) = s_{\mathrm{a}}(-t)$ /* updating source */
4 | | $W_{1p} \leftarrow W_1$; $W_1 \leftarrow W(s_a, [g_{ij}])$
5 | | $[g_{ij}] \leftarrow \underset{[g_{ij}]}{\arg\min}\, W(s_a, [g_{ij}])$ /* updating interferometric transfer functions */
6 | | $W_{2p} \leftarrow W_2$; $W_2 \leftarrow W(s_a, [g_{ij}])$
7 | | $\Delta W = \max(\{W_{1p} - W_1, W_{2p} - W_2\})$ /* measure convergance */
8 | **end**
9 **end**
10 $[\hat{g}_{ij}] \leftarrow [g_{ij}]$; $\hat{s}_a \leftarrow s_a$

Algorithm 2: Focused Phase Retrieval. Solving Y, as in eq. 14, in succession for decreasing values of β. Then solving X in eq. 11.

Preparation
    get the interferometric filters $[\hat{g}_{ij}]$ using FIBD

Parameters (with example)
    $\vec{\beta} = \{\infty, 0\}$
    index of the most front-loaded channel f

Initialize
$$g_i(t) \leftarrow \begin{cases} 0, & \text{if } i = f \text{ and } t \neq 0 \\ \mathrm{rand}(), & \text{otherwise} \end{cases}$$

Results
    filters $[\hat{g}_i]$

Kernel
foreach $\beta \in \vec{\beta}$ **do**   /* loop over decreasing β */
1 | $[g_i] \leftarrow \underset{[g_i]}{\arg\min}\, Y([g_i])$
2 **end**
3 $[g_i] \leftarrow \underset{[g_i]}{\arg\min}\, X([g_i])$ /* return to LSPR */
4 $[\hat{g}_i] \leftarrow [g_i]$
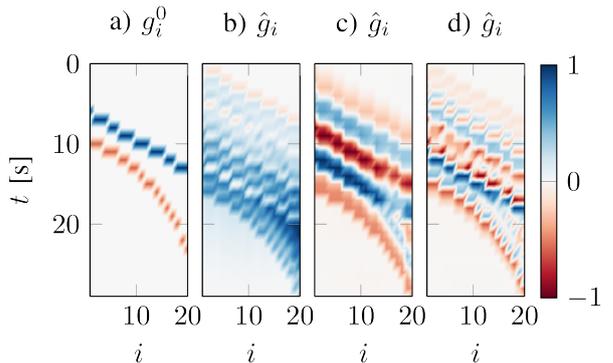
Figure 2: Idealized Experiment I. The results are displayed as images that use the full range of colors in a colormap. Each pixel of these images corresponds to a time t and a channel index i. Impulse responses: a) true; b)—d) undesired.
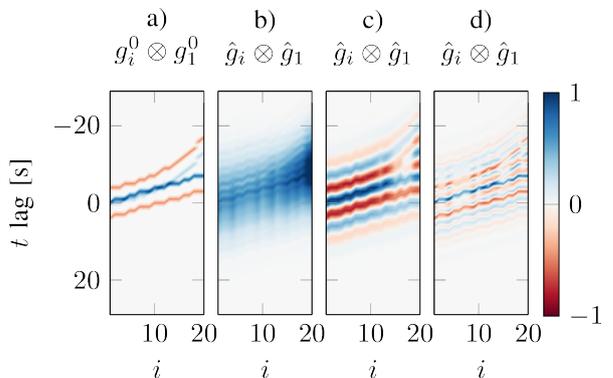
Figure 3: Idealized Experiment I. Cross-correlations of impulse responses corresponding to the Fig. 2: a) true; b)—d) undesired.

the earliest arrival that doesn't undergo scattering. The hyperbolic arrival is likely to represent a wave that is reflected or scattered from an interface between two materials with different acoustic impedances.

LSBD: To illustrate its non-uniqueness, we use three different initial estimates of s and $[g_i]$ to observe the convergence to three different solutions that belong to $\mathbb{P}$. The channel responses corresponding to these solutions are plotted in Figs. 2b–d. At the convergence, the misfit (given in (3)) in all these three cases $U(\hat{s}, [\hat{g}_i]) \lesssim 10^{-6}$, justifying non-uniqueness. Moreover, we notice that none of the solutions is desirable due to insufficient resolution.

FIBD: In order to isolate the indeterminacy due to the amplitude spectrum of the unknown filter $\phi(t)$ in (6) and justify the use of the focusing constraint in (9), we plot the true and undesirable impulse responses after cross-correlation in the Fig. 3. It can be easily noticed that the

Figure 4: Idealized Experiment I. a) FIBD estimated interferometric impulse responses corresponding to the Fig. 3a, after fitting the interferometric channel outputs. b) Same as (a), except after white noise is added to the channel outputs. c) Estimated impulse responses from FPR by fitting the FIBD-outcome interferometric impulse responses in (a). d) Same as (c), except fitting the FIBD outcome in (b).
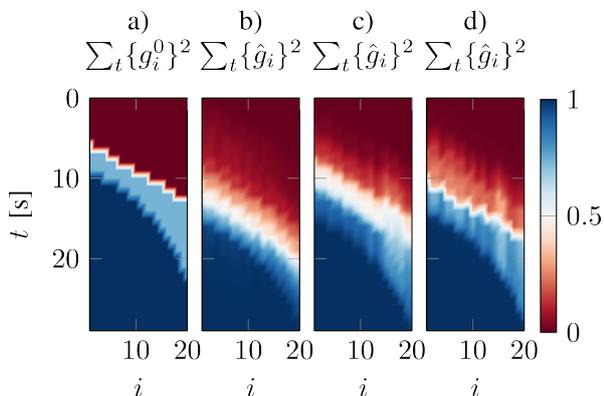
Figure 5: Idealized Experiment I. Normalized cumulative energy of: a) true; b)—d) undesired impulse responses corresponding to the Fig. 2.

true impulse-response cross-correlations corresponding to the first channel are more focused at $t = 0$ than the undesirable impulse-response cross-correlations. The defocusing is caused by the ambiguity related to the amplitude spectrum of $\phi(t)$. FIBD in Algorithm 1 with $\vec{\alpha} = [\infty, 0.0]$ resolves this ambiguity and satisfactorily recovers the true interferometric impulse responses $[g_{ij}^0]$, as plotted in Fig. 4a. We regard the FIBD recovery be satisfactory in Fig. 4b when the Gaussian white noise is added to the channel outputs so that the signal-to-noise (SNR) is $1\,\mathrm{dB}$.

FPR: In order to motivate the use of the second focusing constraint, we plotted the normalized cumulative energy of the true and undesired impulse responses in the Figs. 5. It can be easily noticed that the fastest rate of energy buildup in time occurs in the case of the true impulse responses. In other words, the energy of the true impulse responses is more front-loaded compared to undesired impulse responses, after neglecting an overall translation in time. The FPR in Algorithm 2 with $\vec{\beta} = [\infty, 0]$ satisfactorily recovers $[g_i^0]$ that are plotted in: the Fig. 4c — utilizing $[g_{ij}]$ recovered from the noiseless channel outputs (Fig. 4a); the Fig. 4d — utilizing $[g_{ij}]$ recovered from the channel outputs (Fig. 4b) with Gaussian white noise. Note that the overall time translation and scaling cannot be fundamentally determined.

B. Idealized Experiment II

This IBD-benchmark experiment with $n = 20$ $\tau = 30$ and $T = 400$ aims to reconstruct simpler interferometric impulse responses, plotted in Fig. 6b, corresponding to the true impulse responses in Fig. 6a. A satisfactory recovery of $[g_{ij}^0]$ is not achievable without the focusing constraint — the IBD outcome in the Fig. 6c doesn't match the true interferometric impulse responses in the Fig. 6b, unlike FIBD in the Fig. 6d.

C. Idealized Experiment III

We consider another experiment with $n = 20$ and $\tau = 30$ to reconstruct the true impulse responses $[g_i^0]$ (plotted in Fig. 7a) by fitting their cross-correlations $[g_{ij}^0]$. A satisfactory recovery of $[g_i^0]$ from $[g_{ij}^0]$ is not achievable without the focusing constraint — the outcome of LSPR, in Fig. 7b, doesn't match the true impulse responses, in Fig. 7a, but is contaminated by the filter $\chi(t)$ in (13). On the other hand, FPR results in the outcome (Fig. 7c) that is not contaminated by $\chi(t)$.

D. Idealized Experiment IV

This experiment with $n = 20$, $\tau = 30$ and $T = 400$ aims to reconstruct the true interferometric impulse responses, plotted in Fig. 8b, corresponding to the true impulse responses in Fig. 8a. The outcome of FIBD with $\vec{\alpha} = [\infty, 0]$, plotted in Fig. 8c, doesn't clearly match the true interferometric impulse responses because the channels are *not* sufficiently dissimilar. In this regard, observe that the Fig.-8a true impulse responses at various channels i differ only by a fixed time-translation instead of curving as in Fig. 2a.
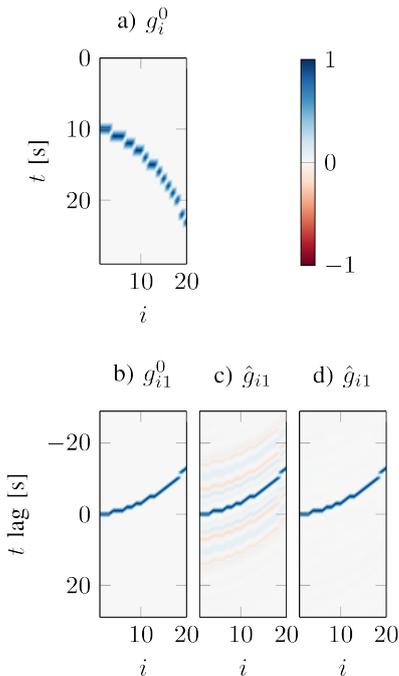
Figure 6: Idealized Experiment II. Interferometric impulse responses: a) true; b) estimated using IBD; c) estimated using FIBD.
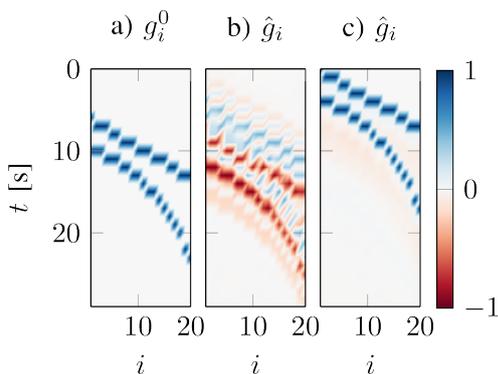
Figure 7: Idealized Experiment III. a) True impulse responses. b) Estimated impulse responses using LSPR. c) Estimated impulse responses using FPR.
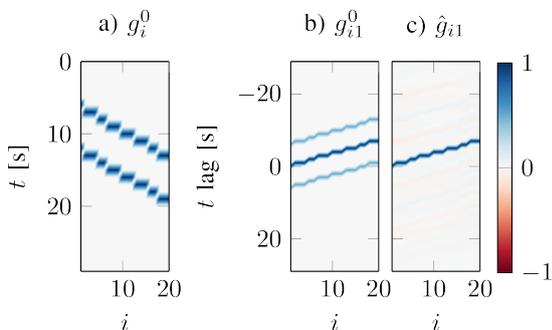
Figure 8: Idealized Experiment IV. a) True impulse responses of channels that are not sufficiently dissimilar. b) True interferometric impulse responses corresponding to (a). c) FIBD estimated interferometric impulse responses corresponding to (b), after fitting the interferometric channel outputs.
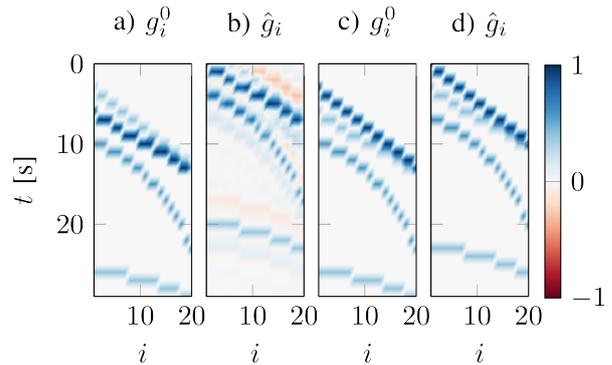
Figure 9: Idealized Experiment V. a) True impulse responses that are not front-loaded. b) FPR estimated impulse responses corresponding to (a), after fitting the true interferometric impulse responses. c) Same as (a), but front-loaded. d) Same as (b), but corresponding to (c).

E. Idealized Experiment V

We consider another experiment with $n = 20$ and $\tau = 30$ to reconstruct the true impulse responses $[g_i^0]$ (plotted in Fig. 9a) that are *not* front-loaded, by fitting their cross-correlations $[g_{ij}^0]$. The FPR estimated impulse responses $[\hat{g}_i]$, plotted in Fig. 9b, do not clearly depict the arrivals because there exists a spurious $\chi \neq \delta$ obeying (13), such that $[g_i^0 * \chi]$ are more front-loaded than $[g_i^0]$. We observe that FPR typically doesn't result in a favorable outcome if the impulse responses are not front-loaded. Otherwise, the front-loaded $[g_i^0]$, plotted in Fig. 9c, are successfully reconstructed in Fig. 9d, except for an overall translation in time.

V. GREEN'S FUNCTION RETRIEVAL

Finally, we consider a more realistic scenario involving seismic-wave propagation in a complex 2-D structural model, which is commonly known as the Marmousi model [62] in exploration seismology. The Marmousi P-wave velocity and impedance plots are in the Figs. 11a and 11b, respectively. We inject an unknown band-limited source signal, e.g., due to a drill bit, into this model for $30\,\mathrm{s}$, such that $T = 3600$. The signal's auto-correlation and power spectrum are plotted in Figs. 10a and 10b, respectively. We used an acoustic time-domain staggered-grid finite-difference solver for wave-equation modeling. The recorded seismic data at twenty receivers spaced roughly $100\,\mathrm{m}$ apart, placed at a depth of roughly $500\,\mathrm{m}$, can be modeled as the output of a linear system that convolves the source signature with the Earth's impulse response, i.e., its Green's function. We recall that in the seismic context:

- the impulse responses $[g_i]$ correspond to the unique subsurface Green's function $g(\vec{x}, t)$ evaluated at the receiver locations $[\vec{x}_i]$, where the seismic-source signals are recorded;
- the channel outputs $[d_i]$ correspond to the noisy subsurface wavefield $d(\vec{x}, t)$ recorded at the receivers only for $\{0, \ldots, T\}$ — we are assuming that
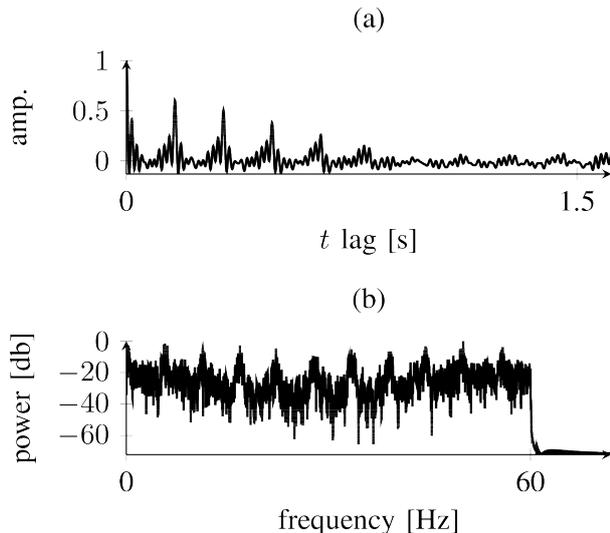
Figure 10: Source signature for the seismic experiment. (a) auto-correlation that contaminates the interferometric Green's functions in the time domain — only 5% of T is plotted; (b) power spectrum, where the Nyquist frequency is 60 Hz.

the source may be arbitrarily on or off throughout this time interval, just as in usual drilling operations;

- τ denotes the propagation time necessary for the seismic energy, including multiple scattering, traveling from the source to a total of n receivers, to decrease below an ad-hoc threshold.

The goal of this experiment is to reconstruct the subsurface Green's function vector $[g_i]$ that contains: 1) the direct arrival from the source to the receivers and 2) the scattered waves from various interfaces in the model. The 'true' Green's functions g_i^0 and the interferometric Green's functions g_{ij}^0, in Figs. 11f and 11c, are generated following these steps: 1) get data for 1.5 s ($\tau = 180$) using a Ricker source wavelet (basically a degree-2 Hermite function modulated to a peak frequency of 20 Hz); 2) create cross-correlated data necessary for $[g_{ij}^0]$; and 3) perform a deterministic deconvolution on the data using the Ricker wavelet. Observe that we have chosen the propagation time to be 1.5 s, such that $T/\tau = 20$.

Seismic interferometry by cross-correlation (see (2)) fails to retrieve direct and the scattered arrivals in the true interferometric Green's functions, as the cross-correlated data $[d_{ij}]$, plotted in Fig. 11d, is contaminated by the auto-correlation of the source signature (Fig. 10a). Therefore, we use FBD to first extract the interferometric Green's functions by FIBD, plotted in the Fig. 11e, and then recover the Green's functions, plotted in the Fig. 11g, using FPR. Notice that the FBD estimated Green's functions clearly depict the direct and the scattered arrivals, confirming that our method doesn't suffer from the complexities in the subsurface models.

VI. Conclusions

Focused blind deconvolution (FBD) solves a series of two optimization problems in order to perform multichannel blind deconvolution (BD), where both the unknown impulse responses and the unknown source signature are estimated given the channel outputs. It is designed for a BD problem where the impulse responses are supposed to be sparse, front-loaded and shorter in duration compared to the channel outputs; as in the case of seismic inversion with a noisy source. The optimization problems use focusing constraints to resolve the indeterminacy inherent to the traditional BD. The first problem considers fitting the interferometric channel outputs and focuses the energy of the impulse-response auto-correlations at the zero lag to estimate the interferometric impulse responses and the source auto-correlation. The second problem completes FBD by fitting the estimated interferometric impulse responses, while focusing the energy of the most front-loaded channel at the zero time. FBD doesn't require any support constraints on the unknowns. We have demonstrated the benefits of FBD using seismic experiments.

APPENDIX A
APPENDIX

In this appendix, we present a simple justification of the ability of a focusing functional on the autocorrelation to select for sparsity, in a setting where ℓ_1 minimization is unable to do so. This setting is the special case of a vector with *nonnegative* entries, made less sparse by convolution with another vector with nonnegative entries as well. This scenario is not fully representative of the more general formulation assumed in this paper, where cancelations may occur because of alternating signs. It seems necessary, however, to make an assumption of no cancelation (like positivity) in order to obtain the type of comparison result that we show in this section.

Consider two infinite sequences f_i and ϕ_j, for $i, j \in \mathbb{Z}$ (the set of integers), with sufficient decay so that all the expressions below make sense, and all the sum swaps are valid. Assume that $f_i \geq 0$ and $\phi_i \geq 0$ for all $i \in \mathbb{Z}$, not identically zero. Let

$$g_j = (f * \phi)_j = \sum_{i \in \mathbb{Z}} f_i \phi_{j-i},$$

which obviously also obeys $g_i \geq 0$ for all $i \in Z$. Assume the normalization condition $\sum_{i \in \mathbb{Z}} \phi_i = 1$.

Now consider the autocorrelations

$$F_j = (f \otimes f)_j = \sum_i f_i f_{j+i},$$

$$G_j = (g \otimes g)_j = \sum_i g_i g_{j+i},$$

and a specific choice of focusing functional,

$$J_F = \sum_{j \in Z} j^2 F_j, \quad J_G = \sum_{j \in \mathbb{Z}} j^2 G_j.$$

Proposition 1.

$$J_G \geq J_F,$$
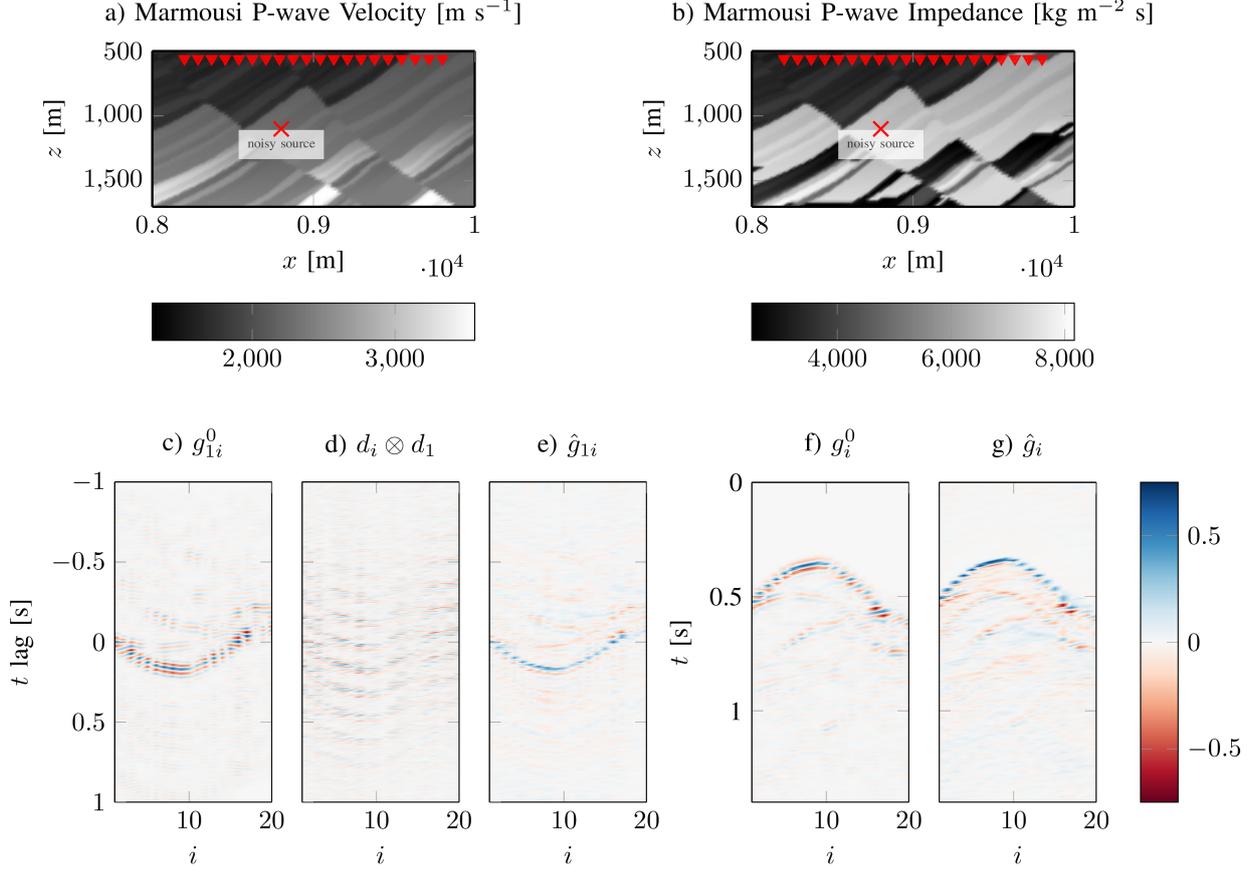
Figure 11: Seismic Experiment. a) Acoustic velocity model for wave propagation. b) Acoustic impedance model depicting interfaces that reflect waves. c) True interferometric Green's functions. d) Seismic interferometry by cross-correlation. e) FIBD estimated interferometric Green's functions. f) True Green's functions. g) FBD estimated Green's functions.

with equality if and only if ϕ_i is the Kronecker δ_{i0}.

Proof. All sums run over $\mathbb{Z}$. Start by observing

$$J_F = \sum_j \sum_k K_{jk} f_j f_k, \qquad K_{jk} = (j-k)^2,$$

and

$$J_G = \sum_j \sum_k L_{jk} f_j f_k,$$

$$L_{jk} = \sum_m \sum_n ((j-k) - (m-n))^2 \phi_m \phi_n.$$

For any particular value $m - n = a$, we have

$$\sum_j \sum_k ((j-k) - a)^2 f_j f_k$$

$$= a^2 \sum_j \sum_k f_j f_k + \sum_j \sum_k (j-k)^2 f_j f_k$$

$$\geq J_F,$$

(the term linear in $j - k$ drops because $j - k$ is antisymmetric in j and k, while $f_j f_k$ is symmetric), with equality if and only if $a = 0$.

Now J_G is a convex combination of such contributions:

$$\sum_m \sum_n \left[\sum_j \sum_k ((j-k) - (m-n))^2 f_j f_k \right] \phi_m \phi_n$$

$$\geq \sum_m \sum_n [J_F] \phi_m \phi_n$$

$$= J_F$$

with equality if and only if the cartesian product supp $\phi \times$ supp ϕ contains only the diagonal $m = n$. This latter scenario only arises when supp $\phi = \{0\}$, which is only compatible with $\sum_i \phi_i = 1$ when $\phi_i = \delta_{i0}$. $\qquad\square$

In contrast, notice that $\sum_i f_i = \sum_i g_i$, hence f and g cannot be discriminated with the ℓ_1 norm. The ℓ_1 norm is unable to measure the extent to which the support of f was "spread" by convolution with ϕ, when $\sum \phi_i = 1$, and when all the functions are nonnegative.

The continuous counterpart of this result, for nonnegative functions $f(t)$ and $g(t) = \int f(s)\phi(t-s)ds$, with nonnegative ϕ such that $\int \phi(t)dt = 1$ in the sense of measures, involves the autocorrelations

$$F(t) = (f \otimes f)(t) = \int f(s)f(s+t)ds,$$

$$G(t) = (g \otimes g)(t),$$

and focusing functionals

$$J_F = \int t^2 F(t)dt, \qquad J_G = \int t^2 G(t)dt.$$

Then, $J_G \geq J_F$, with equality if and only if $\phi(t) = \delta(t)$, the Dirac delta.

ACKNOWLEDGEMENT

REFERENCES

[1] F. Aminzadeh and S. N. Dasgupta, *Geophysics for Petroleum Engineers*. Newnes, 2013, vol. 60.

[2] J. Liu and H. Malvar, "Blind deconvolution of reverberated speech signals via regularization," in *Acoustics, Speech, and Signal Processing, 2001. Proceedings.(ICASSP'01). 2001 IEEE International Conference on*, vol. 5. IEEE, 2001, pp. 3037–3040.

[3] T. Yoshioka, A. Sehr, M. Delcroix, K. Kinoshita, R. Maas, T. Nakatani, and W. Kellermann, "Making machines understand us in reverberant rooms: Robustness against reverberation for automatic speech recognition," *IEEE Signal Processing Magazine*, vol. 29, no. 6, pp. 114–126, 2012.

[4] S.-i. Amari, S. C. Douglas, A. Cichocki, and H. H. Yang, "Multichannel blind deconvolution and equalization using the natural gradient," in *Signal Processing Advances in Wireless Communications, First IEEE Signal Processing Workshop on*. IEEE, 1997, pp. 101–104.

[5] S. C. Douglas, A. Cichocki, and S.-I. Amari, "Multichannel blind separation and deconvolution of sources with arbitrary distributions," in *Neural Networks for Signal Processing [1997] VII. Proceedings of the 1997 IEEE Workshop*. IEEE, 1997, pp. 436–445.

[6] F. Sroubek and J. Flusser, "Multichannel blind iterative image restoration," *IEEE Transactions on Image Processing*, vol. 12, no. 9, pp. 1094–1106, 2003.

[7] P. Bharadwaj, L. Demanet, and A. Fournier, "Focused blind deconvolution of interferometric Green's functions," in *SEG Technical Program Expanded Abstracts*. Society of Exploration Geophysicists, 2018.

[8] G. Xu, H. Liu, L. Tong, and T. Kailath, "A least-squares approach to blind channel identification," *IEEE Transactions on signal processing*, vol. 43, no. 12, pp. 2982–2993, 1995.

[9] S. Subramaniam, A. P. Petropulu, and C. Wendt, "Cepstrum-based deconvolution for speech dereverberation," *IEEE transactions on speech and audio processing*, vol. 4, no. 5, pp. 392–396, 1996.

[10] Y. A. Huang and J. Benesty, "Adaptive multi-channel least mean square and newton algorithms for blind channel identification," *Signal Processing*, vol. 82, no. 8, pp. 1127–1138, 2002.

[11] N. D. Gaubitch, J. Benesty, and P. A. Naylor, "Adaptive common root estimation and the common zeros problem in blind channel identification," in *Signal Processing Conference, 2005 13th European*. IEEE, 2005, pp. 1–4.

[12] A. W. Khong, X. Lin, and P. A. Naylor, "Algorithms for identifying clusters of near-common zeros in multichannel blind system identification and equalization," in *Acoustics, Speech and Signal Processing, 2008. ICASSP 2008. IEEE International Conference on*. IEEE, 2008, pp. 389–392.

[13] D. Kundur and D. Hatzinakos, "Blind image deconvolution," *IEEE signal processing magazine*, vol. 13, no. 3, pp. 43–64, 1996.

[14] P. Campisi and K. Egiazarian, *Blind image deconvolution: theory and applications*. CRC press, 2016.

[15] A. Ahmed, A. Cosse, and L. Demanet, "A convex approach to blind deconvolution with diverse inputs," in *Computational Advances in Multi-Sensor Adaptive Processing (CAMSAP), 2015 IEEE 6th International Workshop on*. IEEE, 2015, pp. 5–8.

[16] X. Li, S. Ling, T. Strohmer, and K. Wei, "Rapid, robust, and reliable blind deconvolution via nonconvex optimization," *arXiv preprint arXiv:1606.04933*, 2016.

[17] A. Ahmed and L. Demanet, "Leveraging diversity and sparsity in blind deconvolution," *arXiv preprint arXiv:1610.06098*, 2016.

[18] J. Romberg, N. Tian, and K. Sabra, "Multichannel blind deconvolution using low rank recovery," in *Independent Component Analyses, Compressive Sampling, Wavelets, Neural Net, Biosystems, and Nanoengineering XI*, vol. 8750. International Society for Optics and Photonics, 2013, p. 87500E.

[19] L. Tong, G. Xu, and T. Kailath, "Blind identification and equalization based on second-order statistics: A time domain approach," *IEEE Transactions on information Theory*, vol. 40, no. 2, pp. 340–349, 1994.

[20] L. Tong, G. Xu, B. Hassibi, and T. Kailath, "Blind channel identification based on second-order statistics: A frequency-domain approach," *IEEE Transactions on Information Theory*, vol. 41, no. 1, pp. 329–334, 1995.

[21] L. Tong and S. Perreau, "Multichannel blind identification: From subspace to maximum likelihood methods," *Proceedings of the IEEE*, vol. 86, no. 10, pp. 1951–1968, 1998.

[22] J. B. Haldorsen, D. E. Miller, and J. J. Walsh, "Walk-away vsp using drill noise as a source," *Geophysics*, vol. 60, no. 4, pp. 978–997, 1995.

[23] T. J. Ulrych, D. R. Velis, and M. D. Sacchi, "Wavelet estimation revisited," *The Leading Edge*, vol. 14, no. 11, pp. 1139–1143, 1995.

[24] X. Liu and H. Liu, "Survey on seismic blind deconvolution," *Progress in Geophysics*, vol. 18, no. 2, pp. 203–209, 2003.

[25] M. Van der Baan and D.-T. Pham, "Robust wavelet estimation and blind deconvolution of noisy surface seismics," *Geophysics*, 2008.

[26] E. A. Robinson, "Predictive decomposition of seismic traces," *Geophysics*, vol. 22, no. 4, pp. 767–778, 1957.

[27] H. Wold, "A study in the analysis of stationary time series," Ph.D. dissertation, Almqvist & Wiksell, 1938.

[28] E. A. Robinson and S. Treitel, *Geophysical signal analysis*. Prentice-Hall Englewood Cliffs, NJ, 1980, vol. 263.

[29] Ö. Yilmaz, *Seismic data analysis*. Society of Exploration Geophysicists Tulsa, 2001, vol. 1.

[30] K. F. Kaaresen and T. Taxt, "Multichannel blind deconvolution of seismic signals," *Geophysics*, vol. 63, no. 6, pp. 2093–2107, 1998.

[31] N. Kazemi and M. D. Sacchi, "Sparse multichannel blind deconvolution," *Geophysics*, vol. 79, no. 5, pp. V143–V152, 2014.

[32] K. Nose-Filho, A. K. Takahata, R. Lopes, and J. M. Romano, "A fast algorithm for sparse multichannel blind deconvolution," *Geophysics*, vol. 81, no. 1, pp. V7–V16, 2015.

[33] E. Liu, N. Iqbal, J. H. McClellan, and A. A. Al-Shuhail, "Sparse blind deconvolution of seismic data via spectral projected-gradient," *arXiv preprint arXiv:1611.03754*, 2016.

[34] N. Kazemi, E. Bongajum, and M. D. Sacchi, "Surface-consistent sparse multichannel blind deconvolution of seismic signals," *IEEE Transactions on geoscience and remote sensing*, vol. 54, no. 6, pp. 3200–3207, 2016.

[35] G. Schuster, J. Yu, J. Sheng, and J. Rickett, "Interferometric/daylight seismic imaging," *Geophysical Journal International*, vol. 157, no. 2, pp. 838–852, 2004.

[36] R. Snieder, "Extracting the greens function from the correlation of coda waves: A derivation based on stationary phase," *Physical Review E*, vol. 69, no. 4, p. 046610, 2004.

[37] N. M. Shapiro, M. Campillo, L. Stehly, and M. H. Ritzwoller, "High-resolution surface-wave tomography from ambient seismic noise," *Science*, vol. 307, no. 5715, pp. 1615–1618, 2005.

[38] K. Wapenaar, E. Slob, and R. Snieder, "Unified greens function retrieval by cross correlation," *Physical Review Letters*, vol. 97, no. 23, p. 234301, 2006.

[39] A. Curtis, P. Gerstoft, H. Sato, R. Snieder, and K. Wapenaar, "Seismic interferometryturning noise into signal," *The Leading Edge*, vol. 25, no. 9, pp. 1082–1092, 2006.

[40] G. T. Schuster, *Seismic interferometry*. Cambridge University Press Cambridge, 2009, vol. 1.

[41] K. Wapenaar and J. Fokkema, "Greens function representations for seismic interferometry," *Geophysics*, vol. 71, no. 4, pp. SI33–SI46, 2006.

[42] J. F. Claerbout, "Synthesis of a layered medium from its acoustic transmission response," *Geophysics*, vol. 33, no. 2, pp. 264–269, 1968.

[43] D. Draganov, K. Wapenaar, and J. Thorbecke, "Seismic interferometry: Reconstructing the earths reflection response," *Geophysics*, vol. 71, no. 4, pp. SI61–SI70, 2006.

[44] L. Borcea, G. Papanicolaou, and C. Tsogka, "Coherent interferometric imaging in clutter," *Geophysics*, vol. 71, no. 4, pp. SI165–SI175, 2006.

[45] L. Demanet and V. Jugnon, "Convex recovery from interferometric measurements," *IEEE Transactions on Computational Imaging*, vol. 3, no. 2, pp. 282–295, 2017.

[46] C. A. Vidal, D. Draganov, J. Van der Neut, G. Drijkoningen, and K. Wapenaar, "Retrieval of reflections from ambient noise using illumination diagnosis," *Geophysical Journal International*, vol. 198, no. 3, pp. 1572–1584, 2014.

[47] C. Gradl, A. W. Eustes, and G. Thonhauser, "An analysis of noise characteristics of drill bits," *Journal of energy resources technology*, vol. 134, no. 1, p. 013103, 2012.

[48] J. Rector III and B. P. Marion, "The use of drill-bit energy as a downhole seismic source," *Geophysics*, vol. 56, no. 5, pp. 628–634, 1991.

[49] B. Joyce, D. Patterson, J. Leggett, and V. Dubinsky, "Introduction of a new omni-directional acoustic system for improved real-time LWD sonic logging-tool design and field test results," in *SPWLA 42nd Annual Logging Symposium*. Society of Petrophysicists and Well-Log Analysts, 2001.

[50] I. Vasconcelos and R. Snieder, "Interferometry by deconvolution: Part 1theory for acoustic waves and numerical examples," *Geophysics*, vol. 73, no. 3, pp. S115–S128, 2008.

[51] R. Snieder and E. Safak, "Extracting the building response using seismic interferometry: Theory and application to the millikan library in pasadena, california," *Bulletin of the Seismological Society of America*, vol. 96, no. 2, pp. 586–598, 2006.

[52] K. Wapenaar, J. van der Neut, and E. Ruigrok, "Passive seismic interferometry by multidimensional deconvolution," *Geophysics*, vol. 73, no. 6, pp. A51–A56, 2008.

[53] K. Wapenaar, J. Van Der Neut, E. Ruigrok, D. Draganov, J. Hunziker, E. Slob, J. Thorbecke, and R. Snieder, "Seismic interferometry by crosscorrelation and by multidimensional deconvolution: A systematic comparison," *Geophysical Journal International*, vol. 185, no. 3, pp. 1335–1364, 2011.

[54] J. van der Neut, J. Thorbecke, K. Mehta, E. Slob, and K. Wapenaar, "Controlled-source interferometric redatuming by crosscorrelation and multidimensional deconvolution in elastic media," *Geophysics*, vol. 76, no. 4, pp. SA63–SA76, 2011.

[55] F. Broggini, R. Snieder, and K. Wapenaar, "Data-driven wavefield focusing and imaging with multidimensional deconvolution: Numerical examples for reflection data with internal multiples," *Geophysics*, vol. 79, no. 3, pp. WA107–WA115, 2014.

[56] S. Makino, H. Sawada, R. Mukai, and S. Araki, "Blind source separation of convolutive mixtures of speech in frequency domain," *IEICE Transactions on Fundamentals of Electronics, Communications and Computer Sciences*, vol. 88, no. 7, pp. 1640–1655, 2005.

[57] P. Bharadwaj, L. Demanet, and A. Fournier, "Deblending random seismic sources via independent component analysis," in *SEG Technical Program Expanded Abstracts*. Society of Exploration Geophysicists, 2017.

[58] G. Ayers and J. C. Dainty, "Iterative blind deconvolution method and its applications," *Optics letters*, vol. 13, no. 7, pp. 547–549, 1988.

[59] F. Sroubek and P. Milanfar, "Robust multichannel blind deconvolution via fast alternating minimization," *IEEE Transactions on Image Processing*, vol. 21, no. 4, pp. 1687–1700, 2012.

[60] L. Vandenberghe and S. Boyd, "Semidefinite programming," *SIAM review*, vol. 38, no. 1, pp. 49–95, 1996.

[61] M. R. Osborne, B. Presnell, and B. A. Turlach, "A new approach to variable selection in least squares problems," *IMA journal of numerical analysis*, vol. 20, no. 3, pp. 389–403, 2000.

[62] A. Brougois, M. Bourget, P. Lailly, M. Poulet, P. Ricarte, and R. Versteeg, "Marmousi, model and data," in *EAEG Workshop-Practical Aspects of Seismic Data Inversion*, 1990.